Available online at www.sciencedirect.com

SciVerse ScienceDirect

Ceramics International 38 (2012) 6341–6347

CERAMICS INTERNATIONAL

www.elsevier.com/locate/ceramint

Hierarchical structured TiO_2 nano-tubes for formaldehyde sensing

Guoqiang Wu[a], Jianwei Zhang[b], Xiaoying Wang[b], Jianjun Liao[c], Hui Xia[d], Sheikh A. Akbar[e], Jianbao Li[c], Shiwei Lin[c,*], Xiaogan Li[b,*], Jing Wang[b]

[a]*State Key Laboratory of Structural Analysis for Industrial Equipment, Dalian University of Technology, Dalian 116024, PR China*
[b]*School of Electronic Science and Technology, Key Lab. of State of Liaoning for Integrated Circuits Technology, Dalian University of Technology, Dalian 116024, PR China*
[c]*Key Laboratory of Ministry of Education for Application Technology of Chemical Materials in Hainan Superior Resources, Hainan University, Haikou 570228, PR China*
[d]*School of Materials Science and Engineering, Nanjing University of Science and Technology, Nanjing, Jiangsu 210094, PR China*
[e]*Center for Industrial Sensors and Measurements (CISM), Department of Materials Science and Engineering, The Ohio State University, Columbus, OH 43210, USA*

Received 25 February 2012; received in revised form 15 April 2012; accepted 1 May 2012
Available online 9 May 2012

Abstract

Hierarchical structured TiO_2 nano-tubes were prepared following a two-step method: the highly ordered uniform TiO_2 nanotube arrays were first grown by the conventional electrochemical anodization of the Ti metal sheet followed by mechanical milling of the as-fabricated TiO_2 nanotube arrays. The obtained nanotubes with a length around 400 nm and opening diameter ~100 nm were formed mixed with the spherical TiO_2 single crystals with a diameter around 10 nm indicating hierarchical nanostructure. The as-synthesized TiO_2 hierarchical nanotubes based resistive-type chemical sensor exhibits good sensitivity to formaldehyde at room temperatures with or without UV-irradiation. The response of the sensor increased almost linearly as a function of the concentration of formaldehyde from 10–50 ppm under UV irradiation. The response of the sensor to different relative humidity and other possible interferents such as ammonia, methanol and alcohol was investigated. The larger response of the sensor to formaldehyde relative to these interferents is suggested to be due to the deeper diffusion of formaldehyde into the TiO_2 nanotubes.

Keywords: TiO_2 nano-tubes; Hierarchical nanostructure; Formaldehyde; Gas sensors

1. Introduction

Nanoporous TiO_2 has attracted great attention due to its unique properties in photocatalysis, energy conversion and storage systems, and chemical sensing [1–10]. Among various nanostructured TiO_2, the nanotubes have more attractive features such as more effective separation of photo-generated electron–hole pair to prevent recombination in solar cells [1–4]. In the TiO_2 nanotubes synthesized by the hydrothermal method [8,9,11,12], cations or protons always exist in between the zigzag Ti–O double layer. Consequently, further high temperature treatment is needed to remove the exchanged protons, which usually lead to undesirable agglomeration of the nanotubes [9,11,12].

In the past, ordered nanotube arrays had been fabricated using the electrochemical anodization process and employed for H_2 gas sensing [5–8]. The splitting of H_2 due to highly active surface sites rendered by the nanotubes and direct interaction between hydrogen and the nanotube surface resulted in a sensor response to various concentrations of hydrogen [5,6]. However, due to the rigidity in the planar structure, the electrode connections for sensors or solar cells are difficult and thus poses a challenge in practical use [4]. Therefore, the porous nanostrutured TiO_2 in the form of particles is still desirable in practical applications.

In this work, the hierarchical structured TiO_2 nano-tubes were innovatively synthesized by a two-step method.

*Corresponding authors. Tel.: +86 411 84706002x8332; fax: +86 411 84706706.
E-mail addresses: linsw@hainu.edu.cn (S. Lin), lixg@dlut.edu.cn (X. Li).

0272-8842/$36.00
http://dx.doi.org/10.1016/j.ceramint.2012.05.004

The crystallography and dimensions at nanoscale were firstly achieved by heat-treatment of the rigid TiO_2 nanotube arrays and the final dispersed nanotubes with predefined nanostructure were obtained independently by mechanical milling. This combined techniques help bypass further high temperature heat-treatment as is usually done in the widely used hydrothermal method to prepare dispersive nanotubes. Sensing properties of the as-synthesized TiO_2 nanotubes based sensors to formaldehyde, a highly health-threatening gas species substantially present both indoors and outdoors [13–17], were demonstrated at room temperature with the assistance of UV illumination.

2. Experimental section

2.1. Materials preparation and microstructure characterization

The two-step process for synthesis of the nanotube-based TiO_2 is schematically illustrated in Fig. 1. During the process, the highly ordered uniform TiO_2 nanotube array was grown by conventional electrochemical anodization of a Ti metal sheet [17]. Titanium sheet (99.4% purity, 0.2 mm thickness) was degreased by ultrasonication for 10 min in acetone, ethanol and deionized water in sequence. The anodization solution was prepared with ethylene glycol (EG) containing 0.3 wt% NH_4F and 2 vol% deionized water. Titanium sheet was anodized at 30 V at room temperature. The electrochemical oxidation occurs on both sides of the Ti sheet and the nanotubes grow towards the middle. Therefore, both ends of the oxide nanotubes would eventually meet each other back-to-back. After anodization, TiO_2 nanotubes were annealed at 400 °C for 2 h. The calcined nanotube arrays were then broken down and ground manually to obtain the TiO_2 nanoparticles with the residual nanotube fragments.

The phase formation of the fabricated samples was analyzed using a powder X-ray diffractometer (XRD: D8 Advance, Bruker- AXS, Germany). The XRD patterns were collected using Ni-filtered Cu K_α radiation at 40 kV and 25 mA between 2θ of 15–65° at a scanning speed of 12°/min. The surface morphology of the fabricated nanotubes was examined using a scanning electron microscope (SEM: S-3000N, Hitachi, Japan) on gold-coated specimens. The more close examination of the microstructure of the samples was further carried out by transmission electron microscopy (TEM: JEOL 2100, Japan).

2.2. Sensor fabrication and electrical measurements

The prepared nanotube-based TiO_2 nanopowders were mixed with alpha-terpineol (Aldrich, Shanghai) forming the printable paste. The paste was then deposited on commercial interdigitated gold electrode printed substrate to form a resistive-type gas sensor following a similar procedure described in Refs. [19,20]. The electrical measurements were conducted in a sealed chamber with a total volume of 50 L [14–17]. The electrical resistance in various gas vapors such as formaldehyde, methanol, ethanol and ammonia in the background of humid ambient (relative humidity (RH)–33–62%) at room temperature (19 ± 3 °C) was measured by an Agilent digital DC electrometer (34401A) with data acquisition capability using the IntuiLink software.

During the sensing measurements, the corresponding gas liquid solutions were injected respectively into the small furnace at the corner. The pure liquid methanol and alcohol were vaporized to prepare the corresponding gases in the chamber. For the formaldehyde and ammonia gas vapor preparations, the concentrated formaldehyde and ammonia aqueous solutions with the concentrations of 40 wt% and 30 wt%, respectively, were used and the water content was deducted when the gas vapor concentrations were calculated. It confirmed that the maximum response induced by the accompanying water generated from the solutions used is around 10% and relatively smaller compared with the targeted formaldehyde analyte as shown in this work. During the recovery to the background, the front window of the chamber was open and the gas vapors left out spontaneously.

The resistance variation of the nanoporous TiO_2 with a change in gas concentration was measured as the sensor signal. The response (R_s) of the sensor is defined as the relative change of the resistance in the ambient background and that in the various analytes: $R_s = (R_a - R_g)/R_a \times 100$, where R_a and R_g are the resistances of the sensor in ambient air and the analytes, respectively. The UV irradiation was conducted by placing a LED light source as close as possible to the top surface of the sensor. The lighting area of the LED was slightly larger than that of the sensor to ensure a full uniform coverage of the light on the sensor surface. The power density of the LED was ~4 mW and the wavelength range was 360–365 nm. This is enough to activate the anatase TiO_2 which has a band gap ~3.2 eV corresponding to a threshold absorption wavelength at 387.5 nm.

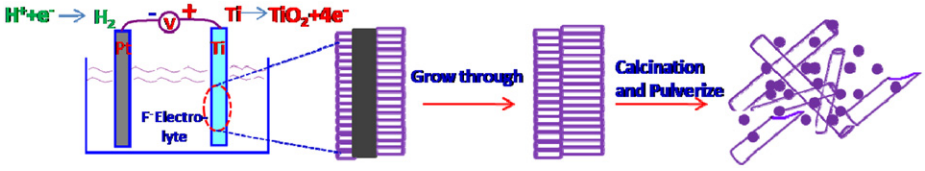

Fig. 1. Schematic of two-step method to synthesize the hierarchical nanotube-based TiO_2.

3. Results and discussion

3.1. Synthesis and characterization of the hierarchical TiO_2 nanotubes

Hierarchical nanostructured TiO_2 nanotubes were synthesized by a two-step method. The highly ordered uniform TiO_2 nanotube array was first grown by conventional electrochemical anodization of a Ti metal sheet followed by mechanical milling. The surface microstructure of the electrochemically anodized TiO_2 nanotube array is shown in Fig. 2(a). The nanotubes were uniformly formed and loosely connected to each other. The contact between the nanotubes is weak and brittle. This allows formation of dispersed nanotubes during the mechanical milling process. The tube diameter in the array is ~120 nm and the wall thickness is ~10–20 nm. After heat treatment of the nanotube arrays at 400 °C for 2 h, the nanotubes had a cleavage in the middle of the nanotubes grown on both sides back-to-back (see Fig. 1). Subsequently, these nanotube arrays were broken down and milled manually for about one hour to achieve the final product.

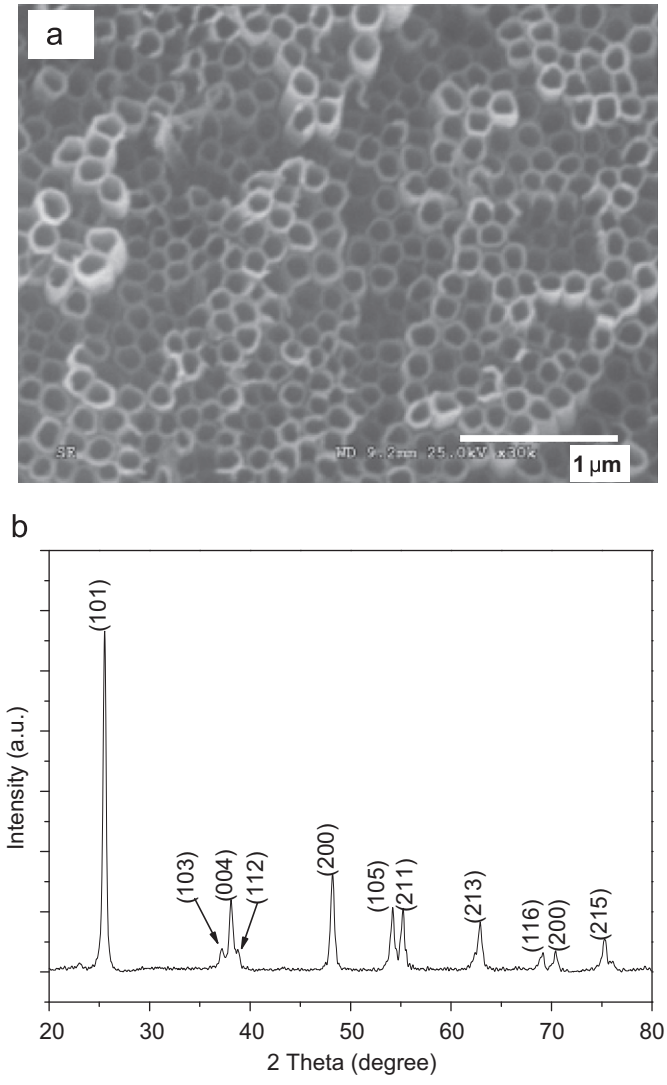

Fig. 2. (a) SEM micrograph and (b) XRD pattern of the surface of as-fabricated TiO_2 nanotube array.

The powder XRD shown in Fig. 2(b) reveals that the final product was an anatase phase. The SEM of the as-prepared TiO_2 nanotube is shown in Fig. 3(a). The sample consists of a mixture of the larger rod-like particles and small aggregates. Therefore, TEM was further conducted to investigate the details of both microstructures. Fig. 3(b) shows the microstructure of the larger porous TiO_2 particles. The clear contrast within a large particle indicates a residual nanotube array fragment which was not completely pulverized during manual grinding.

Fig. 3(c and d) show the detailed features of the small aggregates observed in Fig. 3(a). The small aggregates in reality consisted of two types of particles: the residual broken nanotubes and some nearly spherical nanoparticles. Obviously, one of the two nanotubes in Fig. 3(a) was partly destroyed and left with a half-open tube structure. The other one has an overall tube feature with a length around 400 nm and opening diameter ~100 nm consistent with the SEM result shown in Fig. 2(a). Fig. 3(d) shows that the wall of the nanotubes is "piled-up" with tiny TiO_2 crystals indicating a hierarchical feature of the nanotubes. The hierarchical nanotubes survived the milling process leading to the final nanotube based TiO_2 powders. The loosely bonded hierarchical nanostructure is completely dependent upon the mechanical milling process and bypasses further high temperature heat-treatment as is usually done in the widely used hydrothermal method.

The tiny spherical particles residing along the nanotubes shown in Fig. 3(c) have an average diameter ~10 nm. These nanoparticles came from the broken wall of the nanotubes and are loosely bonded together. Electron diffraction (ED) pattern of these nanoparticles shows that they are single crystals. These combined hierarchical nanostructures are desirable in practical applications such as in gas sensing and solar cells [18,19]. Moreover, in the microstructure of the TiO_2 nanotube arrays shown in Fig. 3(a)–(d), two types of bonding forces can be considered to form the bulk nanotube array as illustrated in Fig. 4. Among them, f_c is the bonding force between the crystals forming on the walls of the nanotubes and f_t is the one between the nanotubes. Therefore, based on the fact that the nanotubes remained as the major phase in the sample after the milling, it can be concluded that the bonding force (f_c) between the tiny crystals on the walls of the nanotubes was slightly stronger than that between the nanotubes (f_t). It can also be anticipated that either the homogeneous nanotube-based or tiny single nanocrystal-based TiO_2 powders can be achieved by appropriately optimizing the milling process.

3.2. Sensing performance of the hierarchical TiO_2 nanotubes based formaldehyde sensor

Fig. 5 shows the response of the hierarchical TiO_2 nanotube-based sensor to 50 ppm formaldehyde in a humid

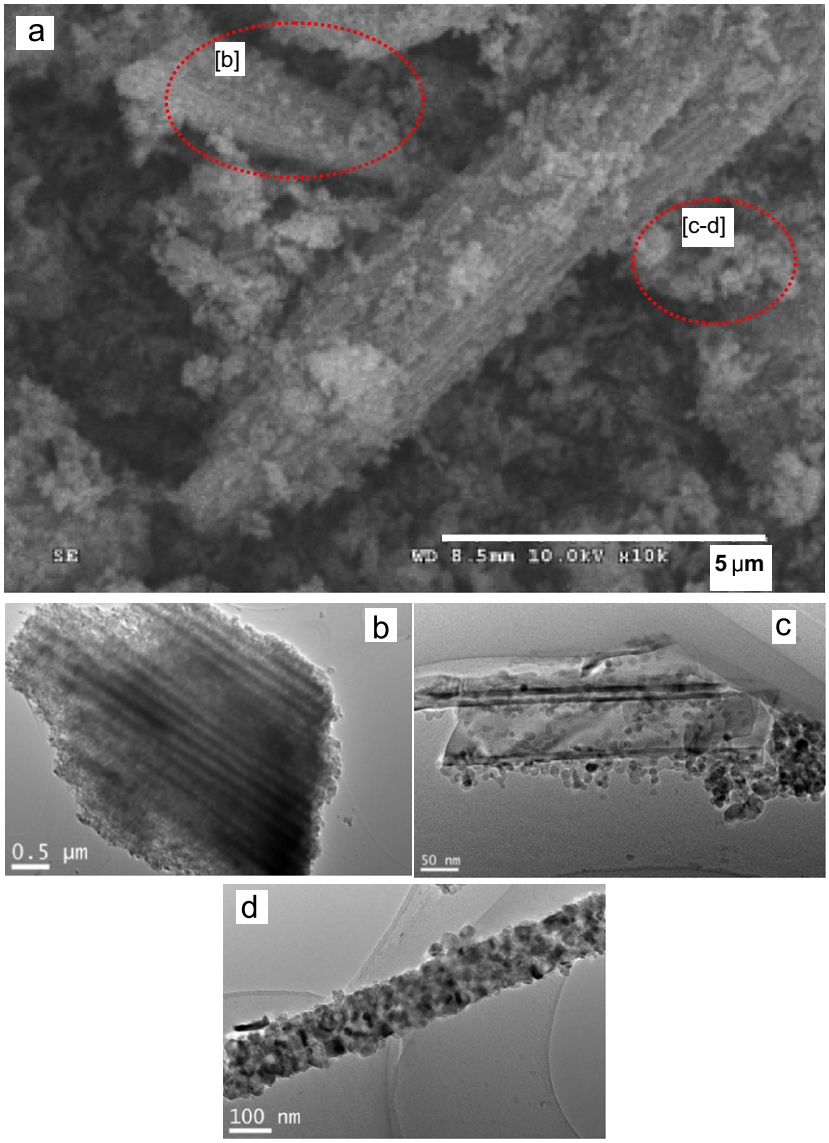

Fig. 3. (a) SEM image of the TiO_2 nanotubes after manually pulverized, (b) and (c) TEM images of the detailed features of the particles in (a), and (d) TEM image of a single TiO_2 nanotube obtained.

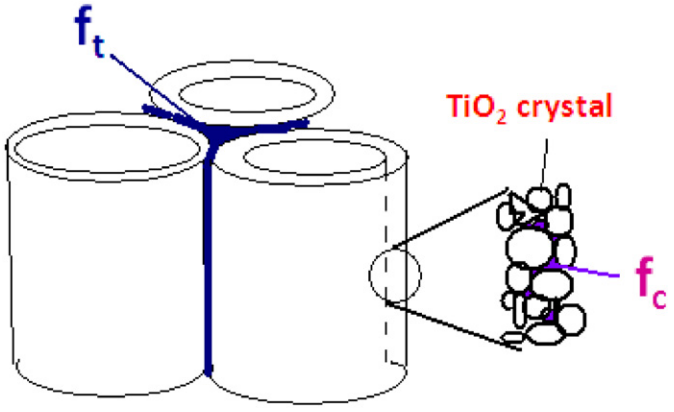

Fig. 4. Illustration of the two types of interfaces, between either nanotubes or nano-particles, in the TiO_2 nanotube arrays.

air (RH: ~62%) at ~19 °C. Anatase TiO_2 is an n-type semiconductor due to the generated oxygen vacancies at the surface releasing the confined electrons. In the TiO_2 nanotubes, the highly defective structure results in a good photocatalytic activity to the adsorbed water which could generate the protons (H^+) leading to a lower resistance and consequently a measurable electronic conductance even at room temperature. Without UV irradiation on the TiO_2 nanotubes, the resistance showed a drift in both ambient and formaldehyde environments (Fig. 5(a)). The resistance of TiO_2 nanoparticles decreased about 2.5% with the introduction of 50 ppm formaldehyde relative to that in the initial humid air. The response/recovery time taken to increase up or decrease down to 90% of the steady-state response was about 3 min and 2 min, respectively.

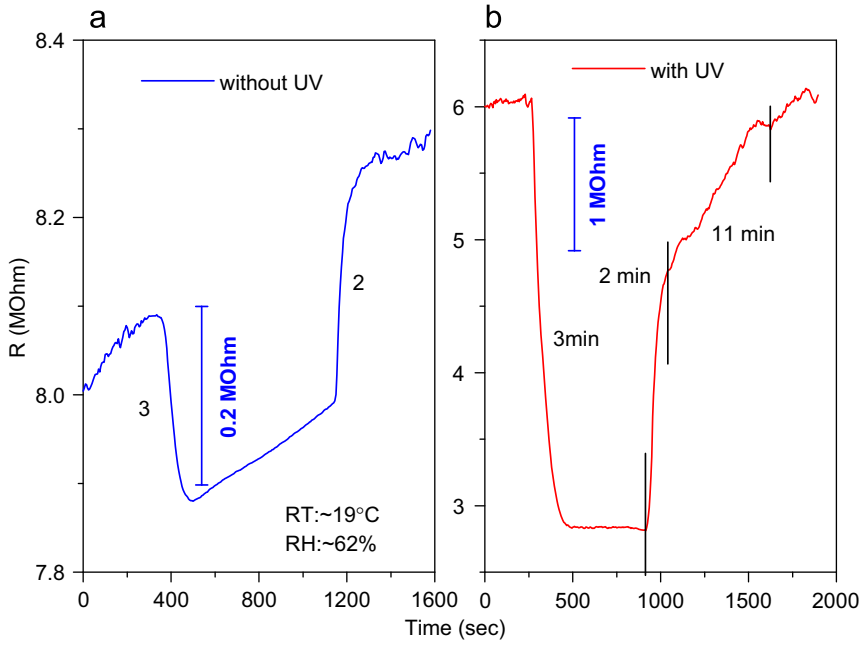

Fig. 5. Response of the TiO_2 nanotube based sensor to ~50 ppm formaldehyde (a) without and (b) with UV irradiation at around 19 °C and RH ~62%.

Under UV irradiation shown in Fig. 5(b), the TiO_2 nanotubes exhibited a more stable resistance and about 50% decrease in 50 ppm formaldehyde. It has been well documented that UV irradiation on nanostructured TiO_2 can excite the electron–hole pair according to following scheme [1–7,2–26]:

$$TiO_2 + hv \rightarrow e^- + h^+ \quad (1)$$

The generated electrons would jump into the conduction band leading to a decrease in the resistance of the bulk [25]. On the other hand, the holes would be extracted to the oxide surface and participate in the chemical oxidative reaction. They split water into the hydroxyl radicals (OH) according to the following reaction [1–7,20–26].

$$H_2O_{(ads)} + h^+ \rightarrow H^+ + \bullet OH \quad (2)$$

These highly active radicals can lead to more active oxidation reaction with formaldehyde according to the reactions [24–27]

$$HCHO + 2\bullet OH \rightarrow CO_2 + H_2O + 2H^+ + 2e^- \quad (3)$$

$$2O^{2-}{}_{(adsorbed)} + 4H^+ \rightarrow 2H_2O \quad (4)$$

Thus, the generated electrons according to reaction (3) led to the strong sensor response in Fig. 5(b).

The response time for the TiO_2 nanotubes under UV irradiation is about 3 min, similar to that in UV-free environment. However, the recovery feature shows much sluggish behavior which is not expected according to literature [24–27]. The recovery curve can be divided into two stages as shown in Fig. 5(b). It takes about 2 min for Stage I to reach a small plateau similar to that in UV-free environment. This stage can be considered as the desorption of part of the products from the surface of TiO_2.

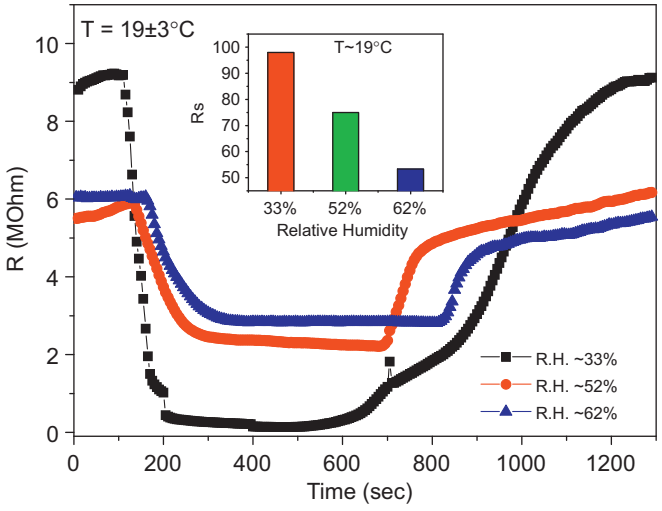

Fig. 6. Humidity influence on the response of the TiO_2 nanotube-based sensor to ~50 ppm formaldehyde at ~19 ± 3 °C with UV irradiation.

However, Stage II takes about 11 min to decrease down to 90% of the steady state response. The exact reason for such sluggish recovery was not clear at the moment. One possible reason might be due to the strongly adsorbed transition products of the formic acid (HCOOH) formed under UV irradiation as reported in Refs. [17,18]. It might take a little longer time for the transition products to be transformed into the final products under UV.

Fig. 6 shows the effect of humidity on the response of the sensor at ~19 °C under the UV irradiation. As observed, the resistance in the air background decreased and the sensor response to 50 ppm formaldehyde also decreased as the humidity increased (inset figure). According to the theory proposed by Hübner et al. based upon the work function

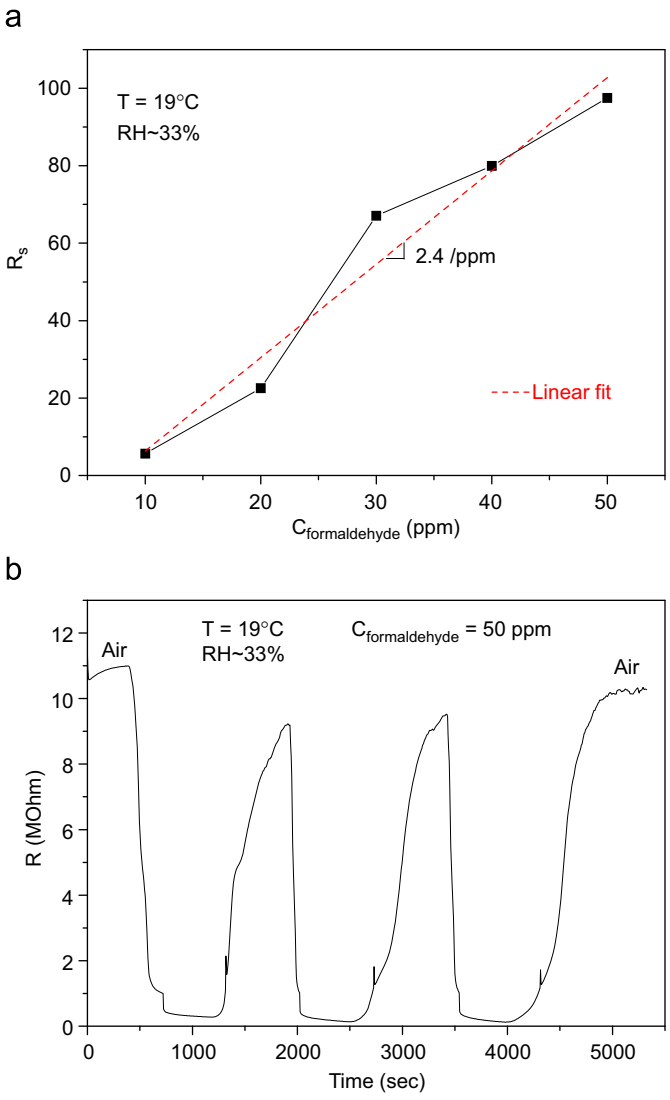

Fig. 7. (a) Sensitivity of the TiO_2 nanotube-based sensor to different concentrations of formaldehyde from 10–50 ppm and (b) reproducibility of the sensor response to 50 ppm formaldehyde at ~19 °C and RH ~33% with UV irradiation.

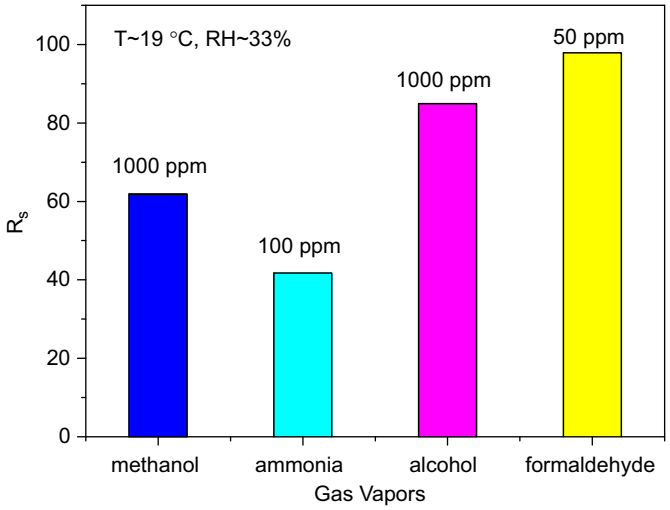

Fig. 8. Comparison of the response of the TiO_2 nanotube based sensor to the four different gas vapors at ~19 °C and RH ~33% with UV irradiation.

measurements, the water vapor would decrease the band bending at the oxide surface thereby leading to an observed decrease in the resistance [28,29]. Moreover, the decrease in the band bending has been attributed to the decrease in the concentration of the chemisorbed oxygen ions at the surface [29]. Consequently, these decreased chemisorbed oxygen ions would decrease the reactions with formaldehyde according to reaction (4), releasing less trapped electrons into the conduction surface of the nanotubes and thus an decrease in the sensor response as observed [28–31].

The sensitivity of the sensor to different concentrations of formaldehyde from 10 to 50 ppm at ~1 °C and RH ~33% under the UV irradiation is shown in Fig. 7(a). The sensor indicates almost a linear increase as the vapor concentration increased. The sensitivity of the sensor defined as the slope of the line is ~2.4. The sensor also shows good stability and reproducibility of the response to 50 ppm formaldehyde as shown in Fig. 7(b).

The response of the nanotube-based TiO_2 sensor to other possible interferents such as ammonia and alcohols under the UV irradiation was further examined. As shown in Fig. 8, the sensor shows the largest response to formaldehyde relative to 100 ppm ammonia, 1000 ppm alcohol and 1000 ppm methanol vapors. Similar results have been found in the nanotube-array based formaldehyde sensor as reported previously [17]. This possibly indicates that formaldehyde polarized with one lone pair in the molecular structure would diffuse deeper into the nanotube causing the larger change in the conductivity. Seo et al. [32] also reported a selective toluene sensor by using hydrothermally obtained TiO_2 nanotubes and it was attributed to the deeper diffusion of the toluene in the nanotubes relative to the interferents. Further studies are needed to understand this interesting observation.

4. Conclusion

The nanotube-based nanoporous TiO_2 were prepared by a two-step method: the rigid highly ordered pure TiO_2 nanotube array was first obtained by using the conventional electrochemical anodization process, followed by mechanical grinding. It is believed that through further optimization of the milling process, more uniform desirable porous nanotube or loosely bonded nanoparticles can be achieved. The highly active surface of the TiO_2 nanotubes significantly enhanced the chemical sensing properties at room temperature with UV irradiation. The response of the sensor increased almost linearly as a function of the concentration of formaldehyde from 10–50 ppm under UV irradiation and demonstrated a higher response compared to other possible interferents such as ammonia, methanol and ethanol. The TiO_2 nanotube-based sensor prepared by this two-step method indicates

potential to be further optimized for a practical formaldehyde detector.

Acknowledgments

The authors would like to thank the financial support from the Fundamental Research Funds for the Central Universities, National Science Foundation of China (Grants Nos. 61001054, 61131004, 61176068), the Program for New Century Excellent Talents in University (NCET-09-0110) and National International Cooperation Program (2009DFA92551).

References

[1] B. O'Regan, M. Gratzel, A low cost, high-efficiency solar cell based on dye-sensitized colloidal TiO_2 films, Nature 353 (1991) 737–740.
[2] O. Carp, C.L. Huisman, A. Reller, Photoinduced reactivity of titanium dioxide, Progress in Solid State Chemistry 32 (2004) 33–177.
[3] K. Hashimoto, H. Irie, A. Fujishima, TiO_2 photocatalysis: a historical overview and future prospects, Japanese Journal of Applied Physics 44 (2005) 8269–8285.
[4] Y. Ji, Z. Tang, Z. Zhang, Z. Zhou, Hydrogen sensing characterizations of titanium dioxide nanotubes, Journal of the Chinese Ceramic Society 36 (2008) 794–798.
[5] C.A. Grimes, Synthesis and application of highly ordered arrays of TiO_2 nanotubes, Journal of Materials Chemistry 17 (2007) 1451–1457.
[6] Y. Li, X. Yu, and Q. Yang, Fabrication of TiO_2 nanotube thin films and their gas sensing properties, Sensors 2009 (2009) 1–19.
[7] G.S. Devi, T. Hyodo, Y. Shimizu, M. Egashira, Synthesis of mesoporous TiO_2-based powders and their gas-sensing properties, Sensors and Actuators B 87 (2002) 122–129.
[8] J.M. Macak, H. Hildebrand, U. Marten-Jahns, P. Schmuki, Mechanistic aspects and growth of large diameter self-organized TiO_2 nanotubes, Journal of Electroanalytical Chemistry 621 (2008) 254–266.
[9] G. Armstrong, R. Armstrong, J. Canales, P.G. Bruce, Nanotubes with the TiO_2-B structure, Chemical Communications (2005) 2454–2456.
[10] S. Yoo, S.A. Akbar, K.H. Sandhage, Nanocarving of bulk titania into oriented arrays single crystal nano-fibers via reaction with hydrogen-bearing gas, Advanced Materials 16 (2004) 260–264.
[11] X. Sun, Y. Li, Synthesis and characterization of ion-exchangeable titanate nanotubes, Chemistry A European Journal 9 (2003) 2229–2238.
[12] X.P. Gao, Y. Lan, H.Y. Zhu, J.W. Liu, Y.P. Ge, F. Wu, D.Y. Song, Electrochemical performance of anatase nanotubes converted from protonated titanate hydrate nanotubes, Electrochemical and Solid-State Letters 8 (2005) A26–A29.
[13] K.C. Gupta, A.G. Ulsamer, P.W. Preuss, Formaldehyde in indoor air: sources and toxicity, Environment International 8 (1982) 349–358.
[14] J. Wang, P. Zhang, J.-Q. Qi, P.-J. Yao, Silicon-based micro-gas sensors for detecting formaldehyde, Sensors and Actuators B 136 (2009) 399–404.
[15] J. Wang, L. Liu, S.-Y. Cong, J.-Q. Qi, B.-K. Xu, An enrichment method to detect low concentration formaldehyde, Sensors and Actuators B 134 (2008) 1010–1015.
[16] P. Lv, Z.A. Tang, J. Yu, F.T. Zhang, G.F. Wei, Z.X. Huang, Y. Hu, Study on a micro-gas sensor with SnO_2–NiO sensitive film for indoor formaldehyde detection, Sensors and Actuators B 132 (2008) 74–80.
[17] S. Lin, D. Li, J. Wu, X. Li, S.A. Akbar, A selective room temperature formaldehyde gas sensor using TiO_2 nanotube arrays, Sensors and Actuators B 156 (2011) 505–509.
[18] Y. Suzuki, Morphology control of TiO_2-based nanomaterials for sustainable energy applications, in: T. Yao (Ed.), Zero-Carbon Energy Kyoto 2009, Springer, Kyoto, 2010, pp. 39–45.
[19] J.-H. Lee, Gas sensors using hierarchical and hollow oxide nanostructures: overview, Sensors and Actuators B 140 (2009) 319–336.
[20] X. Li, R. Ramasamy, P.K. Dutta, Study of the resistance behavior of anatase and rutile thick films towards carbon monoxide and oxygen at high temperatures and possibilities for sensing applications, Sensors and Actuators B 143 (2009) 308–315.
[21] A. Adeyemo, G. Hunter, P.K. Dutta, Interaction of CO with hydrous ruthenium oxide and development of a chemoresistive ambient CO sensor, Sensors and Actuators B 152 (2010) 307–315.
[22] T. Oguchiand, A. Fujishima, Photocatalytic degradation of gaseous formaldehyde using TiO_2 film, Environmental Science and Technology 32 (1998) 3831–3833.
[23] S. Sun, J.J. Ding, J. Bao, C. Gao, Z. Qi, C. Li, Photocatalytic oxidation of gaseous formaldehyde on TiO_2: an in situ DRIFTS study, Catalysis Letters 137 (2010) 239–246.
[24] S.W. Fan, A.K. Srivastava, V.P. Dravid, UV-activated room-temperature gas sensing mechanism of polycrystalline ZnO, Applied Physics Letters 95 (2009) 142106-1-3.
[25] E. Comini, G. Faglia, G. Sberveglieri, UV light activation of tin oxide thin films for NO_2 sensing at low temperatures, Sensors and Actuators B 78 (2001) 73–77.
[26] M. Law, H. Kind, B. Messer, F. Kim, P. Yang, Photochemical sensing of NO_2 with SnO_2 nanoribbon nanosensors at room temperature, Angewandte Chemie International Edition 41 (2002) 2405–2408.
[27] L. Peng, Q. Zhao, D. Wang, J. Zhai, P. Wang, S. Pang, T. Xie, Ultraviolet-assisted gas sensing: a potential formaldehyde detection approach at room temperature based on zinc oxide nanorods, Sensors and Actuators B 136 (2009) 80–85.
[28] N. Barsan, U. Weimar, Understanding the fundamental principles of metal oxide based gas sensors; the example of CO sensing with SnO_2 sensors in the presence of humidity, Journal of Physics: Condensed Matter 15 (2003) 813–839.
[29] M. Hübnera, C.E. Simion, A. Tomescu-Stanoiu, S. Pokhrela, N. Barsana, U. Weimar, Influence of humidity on CO sensing with p-type CuO thick film gas sensors, Sensors and Actuators B 153 (2011) 347–353.
[30] G. Korotcenkova, I. Blinova, V. Brinzaria, J.R. Stetter, Effect of air humidity on gas response of SnO_2 thin film ozone sensors, Sensors and Actuators B 122 (2007) 519–526.
[31] J. Yu, Z.A. Tang, G.Z. Yan, P.C.H. Chan, Z.X. Huang, An experimental study on micro-gas sensors with strip shape tin oxide thin films, Sensors and Actuators B 139 (2009) 346–350.
[32] M.-H. Seo, M. Yuasab, T. Kidab, J.-S. Huhc, N. Yamazoe, K. Shimanoe, Microstructure control of TiO_2 nanotubular films for improved VOC sensing, Sensors and Actuators B 154 (2011) 251–256.